Journal of Sound and Vibration (2000) **229**(2), 411–430
Article No. jsvi.1999.2496, available online at http://www.idealibrary.com on IDEAL®

CALCULATION OF POINT MOBILITIES AT GENERIC MULTI-PLATE/BEAM JUNCTIONS

E. SARRADJ

Institut für Akustik und Sprachkommunikation, Technische Universität Dresden, 01062–Dresden, Germany

(*Received* 14 *September* 1998, *and in final form* 19 *July* 1999)

A new method is presented for the calculation of point mobilities at generic multi-plate/beam junctions. Such a junction is considered to consist of an arbitrary number of semi-infinite plates coupled together through a beam, which may also be omitted. Plates and beams are assumed to obey Mindlin and Timoshenko theories respectively. The calculation is based on a numerical wavenumber integration technique. A specially adapted numerical integration technique is used to reduce the amount of numerical calculations to be done. The method is applied to a number of example structures to test its results and to illustrate its application.

1. INTRODUCTION

The structural dynamic characteristics of source and receiver points are of great importance for both the prediction of power input into a structure and the prediction of structure-borne sound transmission across point junctions in complex built-up structures. The use of point mobilities is an appropriate way to describe these characteristics. In many cases it is impractical, too expensive or even impossible to measure the point mobilities needed for an analysis. Therefore, it may be necessary to calculate or to assess them.

Much work has been done in finding analytical formulations for point mobilities. Cremer and Heckl [1] gave a comprehensive summary of formulas for a number of simple structures, such as beams, plates and shells. Many authors, among them Dyer [2], Eichler [3], Beckmann [4], Heckl [5], Buhlert [6], Ljunggren [7] and Leung and Pinnigton [8], considered various point mobilities of plates in more or less detail. In contrast, very few results are published for point mobilities of more complicated or built-up structures; Lamb [9] and Goyder and White [10] studied beam stiffened plates, while Peterson [11] addressed the point mobility at an intersection of two perpendicular plates. In practice, structures are not likely to be of simple type or to fit one of those rare cases, where formulations for complicated structures are available.

In this situation, one possible way to compute point mobilities is to employ the conventional finite element method (FEM). The structure is then modelled with a number of elements, which are required to be considerably smaller than a typical

0022-460X/00/020411 + 20 $35.00/0

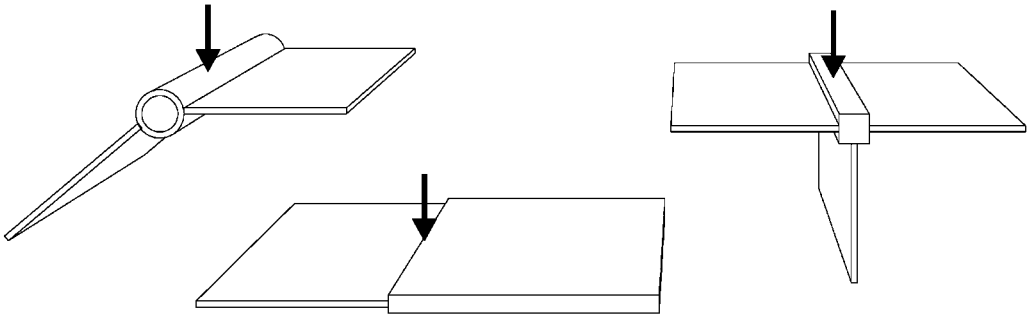

Figure 1. Examples of multi-plate/beam junctions.

wavelength. Thus, as the wavelength becomes smaller with increasing frequency, the required number of elements and the computational effort are growing. This fact restricts the use of this method to low frequencies, where the typical wavelength is not too small compared to the overall dimensions of the structure.

This paper describes a technique to compute point mobilities, that may be applied to a wide range of structures. The amount of numerical computations to be done does not depend on frequency and so, unlike the FEM, the technique can be used also in the high-frequency range. All relevant force and moment mobilities of a point on the connection line of the edges of an arbitrary number of semi-infinite plates are estimated. A stiffening beam along this line may also be taken into account. Figure 1 shows some examples of such junctions.

2. POINT MOBILITIES

In general, a point mobility Y relates a complex transverse or angular velocity (v or w) to a force F or moment M acting on the same point or small area, where the velocity is measured. As the velocity may vary within the small area S_0, some averaging is required to define a "point" mobility. This averaging will be done here on the assumption of equality of the complex power estimated from the velocity and that estimated from the point mobility [12]:

$$P = \frac{1}{2}\int_{S_0} vF''^* \,\mathrm{d}S \equiv P = \frac{1}{2}\,Y_{vF}|F|^2 = \frac{1}{2}\,Y_{vF}\left|\int_{S_0} F''\,\mathrm{d}S\right|^2. \tag{1}$$

The point mobility can be obtained as

$$Y_{vF} = \int_{S_0} vF''^* \,\mathrm{d}S \Big/ \left|\int_{S_0} F''\,\mathrm{d}S\right|^2. \tag{2}$$

The point mobilities Y_{wF}, Y_{vM} and Y_{wM} that are relating an angular velocity to a force or a transverse or angular velocity to a moment, respectively, may be defined on a similar basis.

If all three dimensions are taken into account, a 6×6 point mobility matrix $\mathbf{Y}_P$ has to be considered. It is given by

$$(v_x \; v_y \; v_z \; w_x \; w_y \; w_z)^{\mathrm{T}} = \mathbf{Y}_P \cdot (F_x \; F_y \; F_z \; M_x \; M_y \; M_z)^{\mathrm{T}} \tag{3}$$

As it may be deduced from the reciprocity principle, the matrix $\mathbf{Y}_P$ is symmetric. Consequently, not all the 36, but only 21 elements of the matrix have to be calculated. While in general all elements of the matrix may be non-zero, in many cases practically studied many of them are zero. This is also the case for the considered point on the plate junction and will be discussed later in detail.

3. THEORY

3.1. ARRANGEMENT OF THE PLATES AND THE BEAM AT THE JUNCTION

Figure 2(a) shows a schematic of an example junction of two plates and a beam, which illustrates the type of junction considered here. In general, there may be any number of plates and of course another type of beam. The beam may also be omitted. In global co-ordinates, the x-axis matches the connection line and coincides with the shear axis of the beam. The y-and the z-axis are parallel to the principal axes of the beam cross-section. Therefore, the local co-ordinate system of

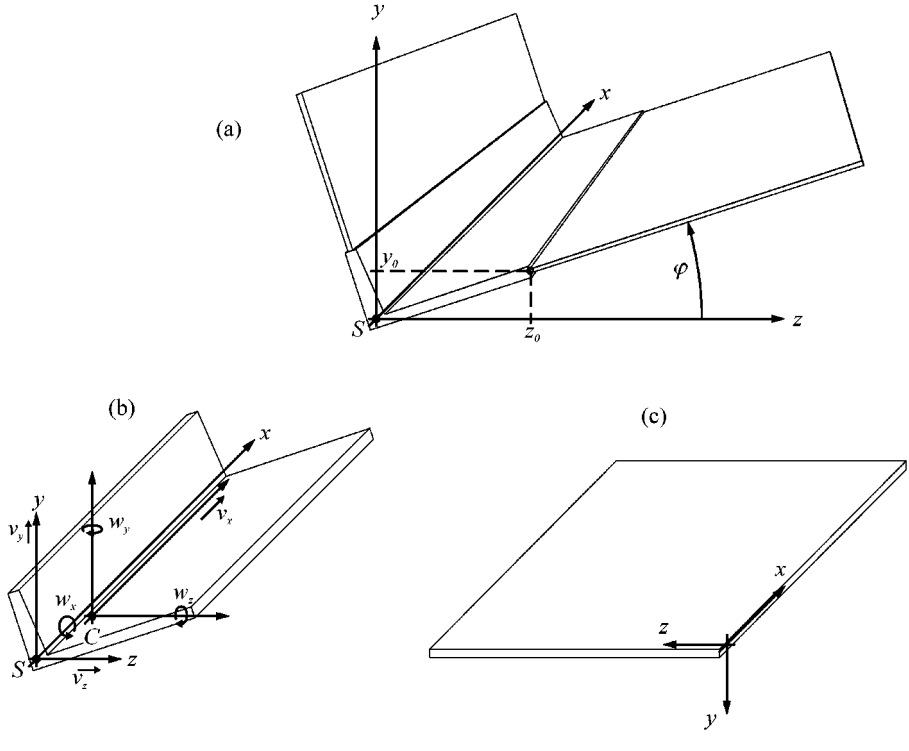

Figure 2. Schematic of plate/beam junction with global co-ordinate system (a) and local co-ordinates for beam (b) and plate (c).

the beam, which is shown in Figure 2(b), does not differ from the global co-ordinate system. The velocities and their corresponding forces and moments are related to the shear centre S in case of v_y, v_z and w_x, while for v_x, w_y and w_z they are related to the centre of gravity $C = (y_C, z_C)$ of the beam cross-section.

The position of each of the semi-infinite plates is given by an angle φ and a possible offset (y_0, z_0) of the connected plate edge. A local co-ordinate system, the x-axis of which coincides with the connected edge, is used for the plates (see Figure 2(c)). The dynamic behaviour of the edge of plate n is fully determined by four independent velocities, $\mathbf{v}_n = (v_x\ v_y\ v_z\ w_x)^{\mathrm{T}}|_{z=0}$ say, and their corresponding forces per unit edge length, $\mathbf{F}'_n = (F'_x\ F'_y\ F'_z\ M'_x)^{\mathrm{T}}|_{z=0}$ say, both of which are given in local co-ordinates.

The velocities of the plate edges must be compatible to the beam velocities (given in global co-ordinates):

$$\mathbf{v}_n = \mathbf{K}_n^{\mathrm{T}}\mathbf{v}_K, \quad \mathbf{v}_K = (v_x \quad v_y \quad v_z \quad w_x \quad w_y \quad w_z)^{\mathrm{T}}|_{(y,\,z)=(0,\,0)}. \tag{4}$$

The matrix $\mathbf{K}_n^{\mathrm{T}}$ for conversion from global to local co-ordinates is given by

$$\mathbf{K}_n^{\mathrm{T}} = \begin{pmatrix} 1 & 0 & 0 & 0 & z_C - z_{0n} & y_{0n} - y_C \\ 0 & \cos\varphi_n & -\sin\varphi_n & y_{0n}\sin\varphi_n + z_{0n}\cos\varphi_n & 0 & 0 \\ 0 & \sin\varphi_n & \cos\varphi_n & z_{0n}\cos\varphi_n - y_{0n}\sin\varphi_n & 0 & 0 \\ 0 & 0 & 0 & 1 & 0 & 0 \end{pmatrix}. \tag{5}$$

The sum of all forces per unit length on the connection line must equate to the external forces per unit length $\mathbf{F}'_e$ applied along the connection line. In global co-ordinates and with the beam forces $\mathbf{F}'_K$ this reads

$$\mathbf{F}'_K + \sum_n \mathbf{K}_n\mathbf{F}'_n = \mathbf{F}'_e. \tag{6}$$

Equations (4) and (6) describe the behaviour of the connection in terms of velocities and forces, respectively. For a full description a link between velocities and forces (and moments) is required, which is provided by the plate edge impedance matrix and the beam impedance matrix. In what follows these matrices will be derived.

3.2. PLATE EDGE IMPEDANCE

A thick plate with linear isotropic behaviour is assumed. The equations of motion for the plate allow for the effects of bending shear and rotatory inertia. Reassembled after reference [1] for reason of the different co-ordinate system and

with a time dependence of $e^{j\omega t}$, they have the form

$$\left(\rho\omega^2 + \frac{E}{1-\mu^2}\frac{\partial^2}{\partial x^2} + G\frac{\partial^2}{\partial z^2}\right)v_x + \frac{1+\mu}{1-\mu}G\frac{\partial^2}{\partial x \partial z}v_z = 0, \tag{7}$$

$$\left(\rho\omega^2 + \frac{E}{1-\mu^2}\frac{\partial^2}{\partial z^2} + G\frac{\partial^2}{\partial x^2}\right)v_z + \frac{1+\mu}{1-\mu}G\frac{\partial^2}{\partial x \partial z}v_x = 0, \tag{8}$$

$$\Delta w_z - \frac{K'}{B'}\left(w_z + \frac{\partial}{\partial x}v_y\right) - \frac{1+\mu}{2}\left(\frac{\partial^2}{\partial z^2}w_z + \frac{\partial^2}{\partial x \partial z}w_x\right) - \omega^2\frac{\Theta''}{B'}w_z = 0, \tag{9}$$

$$\Delta w_x - \frac{K'}{B'}\left(w_x - \frac{\partial}{\partial z}v_y\right) - \frac{1+\mu}{2}\left(\frac{\partial^2}{\partial x^2}w_x + \frac{\partial^2}{\partial x \partial z}w_z\right) - \omega^2\frac{\Theta''}{B'}w_x = 0, \tag{10}$$

$$\frac{\partial}{\partial x}w_z - \frac{\partial}{\partial z}w_x + \left(\Delta - \omega^2\frac{m''}{K'}\right)v_y = 0, \tag{11}$$

where ρ, E, G and μ are the mass density, Young's modulus, shear modulus and Poisson ratio respectively. With the plate thickness h and the shear coefficient κ the quantities $K' = Gh\kappa$, $B' = Eh^3/12(1-\mu^2)$, $\Theta'' = \rho h^3/12$ and $m'' = \rho h$ are given. As it may readily be seen, the first two equations are independent from the others. They determine the in-plane behaviour of the plate. Equations (9)–(11) govern the out-of-plane motion. The elimination of w_x and w_z gives

$$\left(\Delta\Delta + \omega^2\left(\frac{m''}{K'} + \frac{\Theta''}{B'}\right)\Delta - \omega^2\frac{m''}{B'} + \omega^4\frac{m''}{K'}\frac{\Theta''}{B'}\right)v_y = 0. \tag{12}$$

which is the differential equation for bending waves in a thick plate.

With an $e^{jk_x x}e^{jk_z z}$ dependency of all motions assumed, any propagating or evanescent wave must have a wavenumber determined by $k^2 = k_x^2 + k_z^2$. Taking these considerations, equations (7) and (8) yield the wavenumbers for in-plane (longitudinal and transverse) waves

$$k_L^2 = \omega^2\rho(1-\mu^2)/E, \quad k_T^2 = \omega^2\rho/G, \tag{13}$$

while equation (12) gives the wavenumbers for bending waves

$$k_{B1/2}^2 = \frac{k_L^2 + k_{S\kappa}^2}{2} \pm \sqrt{\left(\frac{k_L^2 - k_{S\kappa}^2}{2}\right)^2 + k_{B0}^4}, \tag{14}$$

$$k_{S\kappa}^2 = \omega^2\rho/\kappa G, \quad k_{B0}^4 = \omega^2 m''/B'.$$

The roots of k_{B1}^2 are real and therefore related to a propagating bending wave, while that of k_{B2}^2 are imaginary within the frequency range where equation (12) is valid and consequently related to an evanescent wave.

A plane wave of any type with an amplitude v_0 propagating away from the plate edge at $z = 0$ has a wavenumber k_x, which together with the appropriate wavenumber k for the wave type determines the direction in which the wave is heading. In other words, the wavenumber k_z is given, which must be negative real or positive imaginary for propagating and evanescent waves respectively:

$$k_z = \mathrm{j}\sqrt{k_x^2 - k^2}. \tag{15}$$

Equations (7)–(11), (13) and (14) may be used to derive a relationship between the velocity at the plate edge and the amplitude of all possible wave types:

$$\mathbf{v}_n = \mathbf{C}(v_{L0} \quad v_{T0} \quad v_{B01} \quad v_{B02})^{\mathrm{T}}. \tag{16}$$

The details of the matrix $\mathbf{C}$ are given in Appendix A. Applying Hooke's law and integrating the relevant stresses over the cross-section of the plate edge, the following equations for the forces per unit edge length can be achieved, which must be evaluated at $z = 0$:

$$F_z' = -\int_{-h/2}^{h/2} \sigma_z \,\mathrm{d}y = \frac{\mathrm{j}Eh}{\omega(1-\mu^2)}\left(\mu\frac{\partial}{\partial x}v_x + \frac{\partial}{\partial z}v_z\right), \tag{17}$$

$$F_x' = -\int_{-h/2}^{h/2} \tau_{zx} \,\mathrm{d}y = \frac{\mathrm{j}Gh}{\omega}\left(\frac{\partial}{\partial z}v_x + \frac{\partial}{\partial x}v_z\right), \tag{18}$$

$$M_x' = -\int_{-h/2}^{h/2} \sigma_z y \,\mathrm{d}y = \frac{\mathrm{j}B'}{\omega}\left(\frac{\partial}{\partial z}w_x - \frac{\partial}{\partial x}w_z\right), \tag{19}$$

$$\begin{aligned} F_y' &= -\frac{\partial}{\partial z}M_x' + 2\frac{\partial}{\partial x}\int_{-h/2}^{h/2} \tau_{zx} y \,\mathrm{d}y \\ &= \frac{\mathrm{j}B'}{\omega}\left(\frac{\partial^2}{\partial x \partial z}w_z - (1-\mu)\frac{\partial^2}{\partial x^2}w_x - \frac{\partial^2}{\partial z^2}w_x\right). \end{aligned} \tag{20}$$

With these equations and equations (7)–(11), (13) and (14), after a considerable amount of algebra, it is possible to relate the wave amplitudes to the forces per unit edge length. This relationship may be written in the form

$$\mathbf{F}_n' = \mathbf{Z}_{FM}'(v_{L0} \;\; v_{T0} \;\; v_{B01} \;\; v_{B02})^{\mathrm{T}} \tag{21}$$

with details of the matrix $\mathbf{Z}_{FM}'$ given in Appendix A. Both $\mathbf{C}$ and $\mathbf{Z}_{FM}'$ depend on k_x. Together they yield the plate edge impedance matrix (per unit length)

$$\mathbf{F}_n' = \mathbf{Z}_{EP}'\mathbf{v}_n, \quad \mathbf{Z}_{EP}' = \mathbf{Z}_{FM}'\mathbf{C}^{-1}. \tag{22}$$

It is much more practical to compute the matrix in this form, rather than on a per element basis, as it can easily be done in the case of Kirchhoff plate theory.

3.3. BEAM IMPEDANCE

If a beam is present at the junction, it will oppose motion to any force distribution along the connection line. The equations governing this motion are

$$F'_x = \frac{\mathrm{j}ES_B}{\omega}\frac{\partial^2}{\partial x^2}v_x + \mathrm{j}\omega\rho S_B v_x, \tag{23}$$

$$F'_y = \frac{\mathrm{j}\kappa_y G S_B}{\omega}\left(\frac{\partial^2}{\partial x^2}v_y + \frac{\partial}{\partial x}w_z\right) + \mathrm{j}\omega\rho S_B(v_y - z_C w_x), \tag{24}$$

$$F'_z = \frac{\mathrm{j}\kappa_z G S_B}{\omega}\left(\frac{\partial^2}{\partial x^2}v_z - \frac{\partial}{\partial x}w_y\right) + \mathrm{j}\omega\rho S_B(v_z + y_C w_x), \tag{25}$$

$$M'_x = \frac{\mathrm{j}GJ_{Sx}}{\omega}\frac{\partial^2}{\partial x^2}w_x + \mathrm{j}\omega\rho(S_B(-z_C v_y + y_C v_z) + (I_P + S_B(y_C^2 + z_C^2))w_x), \tag{26}$$

$$M'_y = \frac{\mathrm{j}EI_y}{\omega}\frac{\partial^2}{\partial x^2}w_y + \frac{\mathrm{j}\kappa_z G S_B}{\omega}\left(\frac{\partial}{\partial x}v_z - w_y\right) + \mathrm{j}\omega\rho I_y w_y, \tag{27}$$

$$M'_z = \frac{\mathrm{j}EI_z}{\omega}\frac{\partial^2}{\partial x^2}w_z - \frac{\mathrm{j}\kappa_y G S_B}{\omega}\left(\frac{\partial}{\partial x}v_y + w_z\right) + \mathrm{j}\omega\rho I_z w_z, \tag{28}$$

where S_B and J_{Sx} are the cross-section and the torsional moment about the shear axis, I_P is the polar moment of inertia and I_y and I_z are the second moments of inertia about the y- and the z-axis, respectively. Shear deformation (shear coefficients κ_y, κ_z) and rotatory inertia are taken into account for bending; unlike in reference [13], warping is neglected. With a $\mathrm{e}^{\mathrm{j}k_x x}$ dependence of all motions, an impedance matrix per unit length for the beam can be obtained, which depends on k_x:

$$\mathbf{F}'_K = \mathbf{Z}'_{KB}\mathbf{v}_K \tag{29}$$

(details are given in Appendix B).

3.4. CALCULATION OF THE POINT MOBILITIES

Applying the inverse Fourier transform the ith velocity component on the connection line may be estimated from the corresponding wavenumber spectrum:

$$v_{Ki}(x) = \frac{1}{\sqrt{2\pi}}\int_{-\infty}^{\infty}\breve{v}_{Ki}(k_x)\mathrm{e}^{-\mathrm{j}k_x x}\,\mathrm{d}k_x \tag{30}$$

Equations (4), (6), (22) and (29) provide a relationship between the velocity on the connection and external forces acting:

$$\left(\mathbf{Z}'_{KB} + \sum_n \mathbf{K}_n\mathbf{Z}'_{EP}\mathbf{K}_n^{\mathrm{T}}\right)\mathbf{v}_K = \mathbf{F}'_e. \tag{31}$$

$\mathbf{v}_K$ and $\mathbf{F}'_e$ may be Fourier-transformed to the corresponding quantities in wavenumber space $\breve{\mathbf{v}}_K$ and $\breve{\mathbf{F}}'_e$ respectively so that equation (31) may be rewritten in the form

$$\breve{\mathbf{v}}_K = \mathbf{Y}_K \breve{\mathbf{F}}'_e, \quad \mathbf{Y}_K = \left(\mathbf{Z}'_{KB} + \sum_n \mathbf{K}_n \mathbf{Z}'_{EP} \mathbf{K}_n^{\mathrm{T}} \right)^{-1}. \tag{32}$$

Thus, the velocity components may be written as

$$v_{Ki}(x) = \frac{1}{\sqrt{2\pi}} \int_{-\infty}^{\infty} Y_{Kij} \breve{F}'_{ej} \mathrm{e}^{-\mathrm{j}k_x x} \, \mathrm{d}k_x \tag{33}$$

with F_{ej} denoting the jth component of $\mathbf{F}_e = (F_x \; F_y \; F_z \; M_x \; M_y \; M_z)^{\mathrm{T}}$.

If the stress and therefore the force per unit length are evenly distributed within the excitation area S_0 (with the bounds $(a, -a)$, see Figure 3(b)) and if

$$F_{ej} = \int_{S_0} F''_{ej} \, \mathrm{d}S = \int_{-a}^{a} F'_{ej} \, \mathrm{d}x, \tag{34}$$

which is valid for $j = 1, \ldots, 4$, the force per unit length is given by

$$F'_{ej}(x) = \begin{cases} F_{ej}/2a, & -a < x < a, \\ 0, & \text{otherwise}, \end{cases} \tag{35}$$

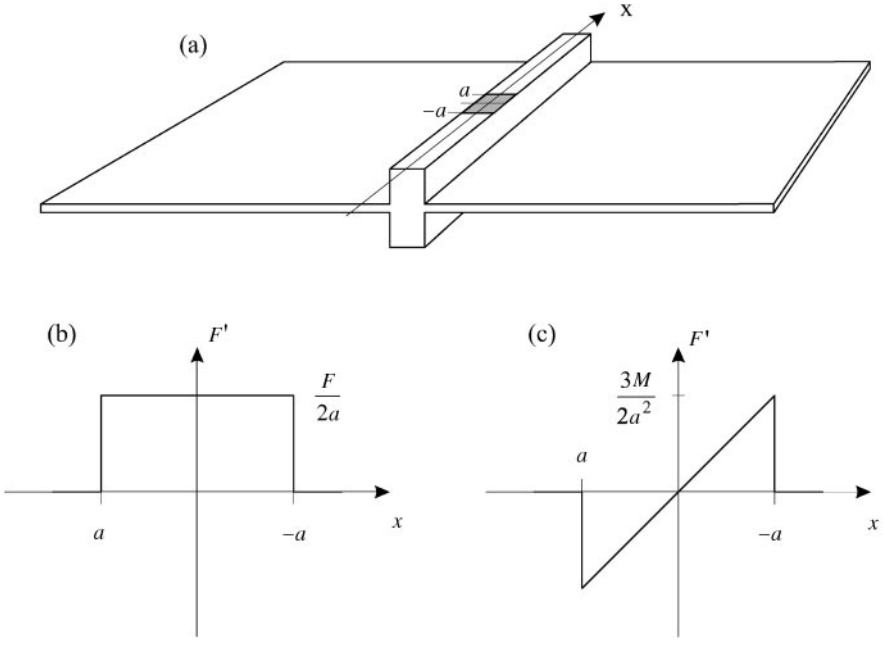

Figure 3. Plate/beam junction with excitation area (a) and stress distribution along the connection line for an acting force (b) and an acting moment (c).

and the corresponding wavenumber spectrum is

$$\breve{F}'_{ej}(k_x) = \frac{1}{\sqrt{2\pi}} \int_{-\infty}^{\infty} F'_{ej}(x) \mathrm{e}^{\mathrm{j}k_x x} \, \mathrm{d}x = \frac{F_{ej}}{\sqrt{2\pi}} \frac{\sin k_x a}{k_x a}. \tag{36}$$

At this point, the definition in equation (2) may be used to calculate the elements of the point mobility matrix:

$$Y_{Pij} = \frac{1}{|F_{ej}|^2} \int_{-a}^{a} \frac{1}{\sqrt{2\pi}} \int_{-\infty}^{\infty} Y_{Kij} \breve{F}'_{ej} \mathrm{e}^{-\mathrm{j}k_x x} \, \mathrm{d}k_x \cdot F'^{*}_{ej} \, \mathrm{d}x. \tag{37}$$

If the expression to integrate is an even function of k_x it may be sufficient to integrate within the bounds $(0, \infty)$ only, but if the function is odd the integral evaluates to zero. Equation (37) is simplified to give

$$Y_{Pij} = \begin{cases} \dfrac{1}{\pi} \displaystyle\int_0^{\infty} Y_{Kij} \left(\frac{\sin k_x a}{k_x a} \right)^2 \mathrm{d}k_x, & \text{if } Y_{Kij}(k_x) = Y_{Kij}(-k_x), \\ 0, & \text{if } Y_{Kij}(k_x) = -Y_{Kij}(-k_x), \end{cases} \qquad i, j = 1, \ldots, 4. \tag{38}$$

It is emphasized that the above calculation may only be used for mobilities that relate one of the forces F_x, F_y, F_z or the moment M_x (corresponding to the indices 1–4) to the associated one of the velocities v_x, v_y, v_z of w_x. For the remaining moments M_y, M_z and angular velocities w_y, w_z the basis for the calculation is the definition

$$Y_{wM} = \int_{-a}^{a} vF'^{*} \, \mathrm{d}x \Big/ \left| \int_{-a}^{a} F'x \, \mathrm{d}x \right|^2. \tag{39}$$

For the sake of simplicity, a linear stress distribution within the excitation area is assumed. Other possible forms of stress distributions do not lead to remarkably different results, unless the frequency is outside the limits of the underlying plate and beam theory, where effects such as volumetric near fields [14] have to be taken into account. With

$$M_{z/y} = \int_{-a}^{a} \pm F'_{y/z} x \, \mathrm{d}x \tag{40}$$

the forces per unit length are

$$F'_{y/z}(x) = \begin{cases} \pm 3M_{z/y} x / 2a^3, & -a < x < a \\ 0, & \text{otherwise} \end{cases} \tag{41}$$

(see Figure 3(c)), leading to the wavenumber spectra

$$\breve{F}'_{y/z} = \pm \mathrm{j} \frac{3M_{z/y}}{2a^3} \frac{1}{k_x a} \left(\frac{\sin k_x a}{k_x a} - \cos k_x a \right). \tag{42}$$

Under the same conditions as for equation (38) the point mobilities are

$$Y_{Pij} = \begin{cases} \dfrac{9}{\pi a^2} \displaystyle\int_0^\infty Y_{K(8-i)(8-j)} \left(\frac{1}{k_x a}\right)^2 \left(\frac{\sin k_x a}{k_x a} - \cos k_x a\right)^2 \mathrm{d}k_x & i, j = 5, 6. \\ 0 \end{cases} \quad (43)$$

The remaining elements of the point mobility matrix relate the moments M_y and M_z to v_x, v_y, v_z or w_x and F_x, F_y, F_z or M_x to w_y and w_z, respectively. Using suitable equations similar to equations (2) and (39) for all these elements it is required to integrate an odd function within symmetric bounds; consequently, they all evaluate to zero. This result is also provided by the following consideration: M_y and M_z are acting about axes which are lying in the symmetry plane of the plate junction and crossing the centre of gravity C of the beam cross-section. If it is recognized that there is no resulting translation of C at $x = 0$, the velocity v_x, which is related to C, must be zero. Further, the local distribution of the resulting velocities v_y, v_z or w_x, all of which are related to the shear centre S, must be an odd function of x, having the value 0 for $x = 0$. Similar arguments apply in the case of F_x. Thus, all point mobilities relate to either F_x or v_x do vanish.

4. NUMERICAL IMPLEMENTATION

A summary of the above considerations shows, for the point mobility matrix,

$$\mathbf{Y}_P = \begin{pmatrix} Y_{P11} & 0 & 0 & 0 & 0 & 0 \\ & Y_{P22} & Y_{P23} & Y_{P24} & 0 & 0 \\ & & Y_{P33} & Y_{P34} & 0 & 0 \\ & & & Y_{P44} & 0 & 0 \\ & \text{symm.} & & & Y_{P55} & Y_{P56} \\ & & & & & Y_{P66} \end{pmatrix} \quad (44)$$

only 10 elements that must be estimated either from equations (38) or (43).

The integrals to be solved for this end must be computed numerically because the mobilities $Y_{Kij}(k_x)$ are computed by using a (numerical) matrix inversion as shown in equation (32). However, this is not always possible since the integrand may have singularities on the real axis. The position of these singularities cannot be estimated exactly, so it is impracticable to calculate the value of the integral using residues. A small artificial damping introduced for the wavenumber to render it complex [1] and to shift the possible singularities off the real axis enables the numerical computation of the integral. Nevertheless, such a computation requires a great number of function values to be estimated and is therefore not very efficient. In what follows an alternative way is proposed.

The $Y_{Kij}(k_x)$ are interpolated by rational functions $g_{ij}(k_x)$, the function values of which may be computed with much less computational effort. Since $Y_{Kij}(k_x)$ always

vanishes if $k_x \to \infty$, the interpolating rational function must do so and consequently must have the form

$$g_{ij}(k_x) = \sum_{m=0}^{p} a_m k_x^m \Big/ \sum_{n=0}^{q} b_n k_x^n, \tag{45}$$

where the degree p of the polynomial in the numerator is lower than the degree q of the polynomial in the denominator. The function $Y_{Kij}(k_x)$ has to be evaluated only $(p + q + 1)$ times to compute all the coefficients a_m and b_n rather than several hundred times for the numerical integration. The higher the degree of the polynomials is, the better is theoretically the approximation of the integrals. However, in practice, the values of $Y_{Kij}(k_x)$ used to estimate the coefficients can only be estimated with limited precision and so p and q chosen too high will cause numerical errors. An illustration of this behaviour is shown in the next section. For the sake of brevity, further details of the interpolation algorithm as well as the numerical integration will not be considered here. The interested reader is referred to the literature (e.g. references [15,16]).

5. EXAMPLE APPLICATIONS

5.1. INFINITE PLATE

An infinite plate may also be seen as a pseudo-junction of two semi-infinite plates with a subtended angle of 180°. Thus, the point mobilities on the junction line between these plates are equivalent to those of an infinite plate. Since analytical results are available for all point mobilities, the case of an infinite plate is a suitable probe of the numerical algorithm.

Only slightly different results for the point force mobility for an in-plane force acting on a rigid circular indenter can be found in references [4, 7, 8]. Reference [7] also provides the point moment mobility for a moment acting around an axis perpendicular to the plate. The classical out-of-plane point force and point moment mobility are calculated in reference [6] and [2], respectively. In both references [2, 6] Mindlin plate theory is employed. For a radius a of the indenter the mobilities are

$$Y_{P11} = Y_{P33} = \frac{\omega}{4Gh}\left(\frac{(3-\mu)}{4} + \mathrm{j}\left(\frac{1-\mu}{2\pi}\ln\frac{2}{k_L a} + \frac{1}{\pi}\ln\frac{2}{k_T a}\right)\right), \tag{46}$$

$$Y_{P22} = \frac{\omega A}{2a\sqrt{(k_L^2 - k_{S\kappa}^2)^2 + 4k_{B0}^4}}\left(\frac{1 + Bk_{B1}^2}{k_{B1}}\left(\mathrm{J}_1(k_{B1}a) - \mathrm{jN}_1(k_{B1}a) - \frac{2\mathrm{j}}{\pi k_{B1}a}\right)\right.$$

$$\left. - \frac{1 + Bk_{B2}^2}{k_{B2}}\left(\mathrm{J}_1(k_{B2}a) - \mathrm{jN}_1(k_{B2}a) - \frac{2\mathrm{j}}{\pi k_{B2}a}\right)\right), \tag{47}$$

$$A = (1 - \omega^2\rho h^2\kappa/12G)/B', \quad B = B'\kappa/Gh(1 - \omega^2\rho h^2\kappa/12G)$$

(J_1 and N_1 denoting the Bessel and Neumann functions of first order, respectively)

$$Y_{P44} = Y_{P66} = \frac{\omega}{4\pi B'}\left(\frac{\pi}{4} + \mathrm{j}\left(\frac{4}{1-\mu}\left(\frac{h}{\pi a}\right)^2 - \ln k_{B1} a\right)\right), \tag{48}$$

$$Y_{P55} = \frac{\omega}{4Gh}\left(\frac{k_T^2}{4} + \mathrm{j}\,\frac{1}{\pi a^2}\right). \tag{49}$$

The remaining elements of the point mobility matrix are zero.

Table 1 shows the results for an infinite steel plate ($E = 2{\cdot}1$ GPa, $\rho = 7800$ kg/m^3, $\mu = 0{\cdot}3$, $h = 2$ mm). The parameter a was chosen to be 5 mm. The numerical values for the real parts agree remarkably well with those obtained from equations (46)–(49). A likely reason for the differences in the imaginary parts is the different shape of the indenter. In equations (46)–(49) a circular indenter with radius a is assumed, while a linear indenter with length $2a$ is considered in the case of the numerically estimated point mobility of the junction.

As already mentioned, the quality of the results estimated numerically relies on the degree of the interpolating functions. Table 2 shows this dependency for the case of the infinite plate. Interpolating polynomials of high degree result in a more accurate estimation of the mobility than those of lower degrees. With interpolating functions of a very high degree ($p = 11$, $q = 12$ in this case), the result becomes erroneous due to numerical errors (A machine precision of 16 digits was used). Although $p = 10$, $q = 11$ give the best results in the case of the infinite plate considered here, interpolating functions of the same high degree cause already large numerical errors due to relatively imprecise estimation of the values of $Y_{Kij}(k_x)$ for

TABLE 1

Point mobilities for an infinite steel plate (*see text for parameters*) *in m/N s and 1/m N s respectively*

		100 Hz	1 kHz	10 kHz
Y_{P11}	(46)	$6{\cdot}56\times10^{-7} + 3{\cdot}24\times10^{-6}$ j	$6{\cdot}56\times10^{-6} + 2{\cdot}28\times10^{-5}$ j	$6{\cdot}56\times10^{-5} + 1{\cdot}32\times10^{-4}$ j
	Num	$6{\cdot}56\times10^{-7} + 2{\cdot}08\times10^{-6}$ j	$6{\cdot}56\times10^{-6} + 2{\cdot}07\times10^{-5}$ j	$6{\cdot}56\times10^{-5} + 1{\cdot}51\times10^{-4}$ j
Y_{P22}	(47)	$2{\cdot}55\times10^{-3} - 5{\cdot}97\times10^{-6}$ j	$2{\cdot}54\times10^{-3} - 4{\cdot}49\times10^{-5}$ j	$2{\cdot}45\times10^{-3} - 3{\cdot}00\times10^{-4}$ j
	Num.	$2{\cdot}53\times10^{-3} - 1{\cdot}88\times10^{-4}$ j	$2{\cdot}51\times10^{-3} - 2{\cdot}30\times10^{-4}$ j	$2{\cdot}38\times10^{-3} - 4{\cdot}50\times10^{-4}$ j
Y_{P33}	(46)	$6{\cdot}56\times10^{-7} + 3{\cdot}24\times10^{-6}$ j	$6{\cdot}56\times10^{-6} + 2{\cdot}28\times10^{-5}$ j	$6{\cdot}56\times10^{-5} + 1{\cdot}32\times10^{-4}$ j
	Num.	$6{\cdot}48\times10^{-7} + 1{\cdot}82\times10^{-6}$ j	$6{\cdot}45\times10^{-6} + 1{\cdot}80\times10^{-5}$ j	$6{\cdot}44\times10^{-5} + 1{\cdot}23\times10^{-4}$ j
Y_{P44}	(48)	$0{\cdot}255 + 0{\cdot}891$ j	$2{\cdot}55 + 5{\cdot}17$ j	$25{\cdot}5 + 14{\cdot}0$ j
	Num.	$0{\cdot}255 + 1{\cdot}34$ j	$2{\cdot}54 + 9{\cdot}76$ j	$24{\cdot}2 + 60{\cdot}4$ j
Y_{P55}	(49)	$9{\cdot}27\times10^{-9} + 0{\cdot}0124$ j	$9{\cdot}27\times10^{-6} + 0{\cdot}124$ j	$9{\cdot}27\times10^{-3} + 1{\cdot}24$ j
	Num.	$1{\cdot}42\times10^{-8} + 1{\cdot}99\times10^{-5}$ j	$1{\cdot}40\times10^{-5} + 0{\cdot}0195$ j	$0{\cdot}0140 + 3{\cdot}61$ j
Y_{P66}	(48)	$0{\cdot}255 + 0{\cdot}891$ j	$2{\cdot}55 + 5{\cdot}17$ j	$25{\cdot}5 + 14{\cdot}0$ j
	Num.	$0{\cdot}250 + 1{\cdot}10$ j	$2{\cdot}49 + 7{\cdot}35$ j	$24{\cdot}0 + 36.4$ j

TABLE 2

Dependency of the results for the point mobility Y_{P22} for an infinite steel plate from the degree p, q of the interpolating polynomials ($f = 100\,Hz$; see text for plate parameters)

p	q	Y_{P22} (m/Ns)	Remarks
1	2	$2{\cdot}205 \times 10^{-3} - 3{\cdot}709 \times 10^{-2}\,\mathrm{j}$	
2	3	$2{\cdot}390 \times 10^{-3} - 2{\cdot}066 \times 10^{-2}\,\mathrm{j}$	
3	4	$2{\cdot}414 \times 10^{-3} - 1{\cdot}888 \times 10^{-4}\,\mathrm{j}$	
4	5	$2{\cdot}468 \times 10^{-3} - 2{\cdot}053 \times 10^{-4}\,\mathrm{j}$	
5	6	$2{\cdot}488 \times 10^{-3} - 2{\cdot}076 \times 10^{-4}\,\mathrm{j}$	
6	7	$2{\cdot}512 \times 10^{-3} - 1{\cdot}875 \times 10^{-4}\,\mathrm{j}$	
7	8	$2{\cdot}525 \times 10^{-3} - 1{\cdot}878 \times 10^{-4}\,\mathrm{j}$	This p, q were used for computations
8	9	$2{\cdot}535 \times 10^{-3} - 1{\cdot}878 \times 10^{-4}\,\mathrm{j}$	
9	10	$2{\cdot}543 \times 10^{-3} - 1{\cdot}875 \times 10^{-4}\,\mathrm{j}$	
10	11	$2{\cdot}550 \times 10^{-3} - 1{\cdot}876 \times 10^{-4}\,\mathrm{j}$	Best agreement of the real part with equation (47)
11	12	$2{\cdot}565 \times 10^{-3} - 1{\cdot}875 \times 10^{-4}\,\mathrm{j}$	Small error due to computational precision
12	13	$7{\cdot}565 \times 10^{-1} - 23{\cdot}88$	Large error—result not meaningful
13	14		No result—division by zero error

other configurations. This depends mainly on the condition of the inverse of $\mathbf{Y}_k$ from equation (32). Low values of p and q lead to completely inaccurate results for most configurations. Therefore, interpolating functions of degrees $p = 7$, $q = 8$, which have shown to be the best possible compromise, were used for all the examples in this and in the next section.

The influence of a on the out-of-plane point force mobility is shown in Figure 4. Both the real and the imaginary parts of the mobility are shown for different values of a. The numerical and the analytical results from equation (47) are normalized by the plate point mobility according to simple bending theory ($Y_0 = 1/8\sqrt{B'm''}$) [1]. The real part results are in very good agreement for all values of a. The small difference which remains even at low frequencies would vanish if interpolating functions of higher degree were used (see Table 2). Despite a common trend it is obvious that there is an offset between the analytical and the numerical results for the imaginary part. The reason for this is related to the different shape of the indenter already mentioned above. Nevertheless, for both analytical and numerical results in the low-frequency range the mobility does nearly not depend on frequency or on a. Moreover, the larger the value of a is, the stronger is the variation of both real and imaginary parts with increasing frequency.

5.2. BEAM-STIFFENED PLATE AND T-PLATE

While the simple case of an infinite plate was selected mainly for benchmark purposes, more complicated built-up structures are included here to yield results from the numerical algorithm that cannot (or only in part) be calculated analytically. The first type of structure, a beam-stiffened plate, was already subject

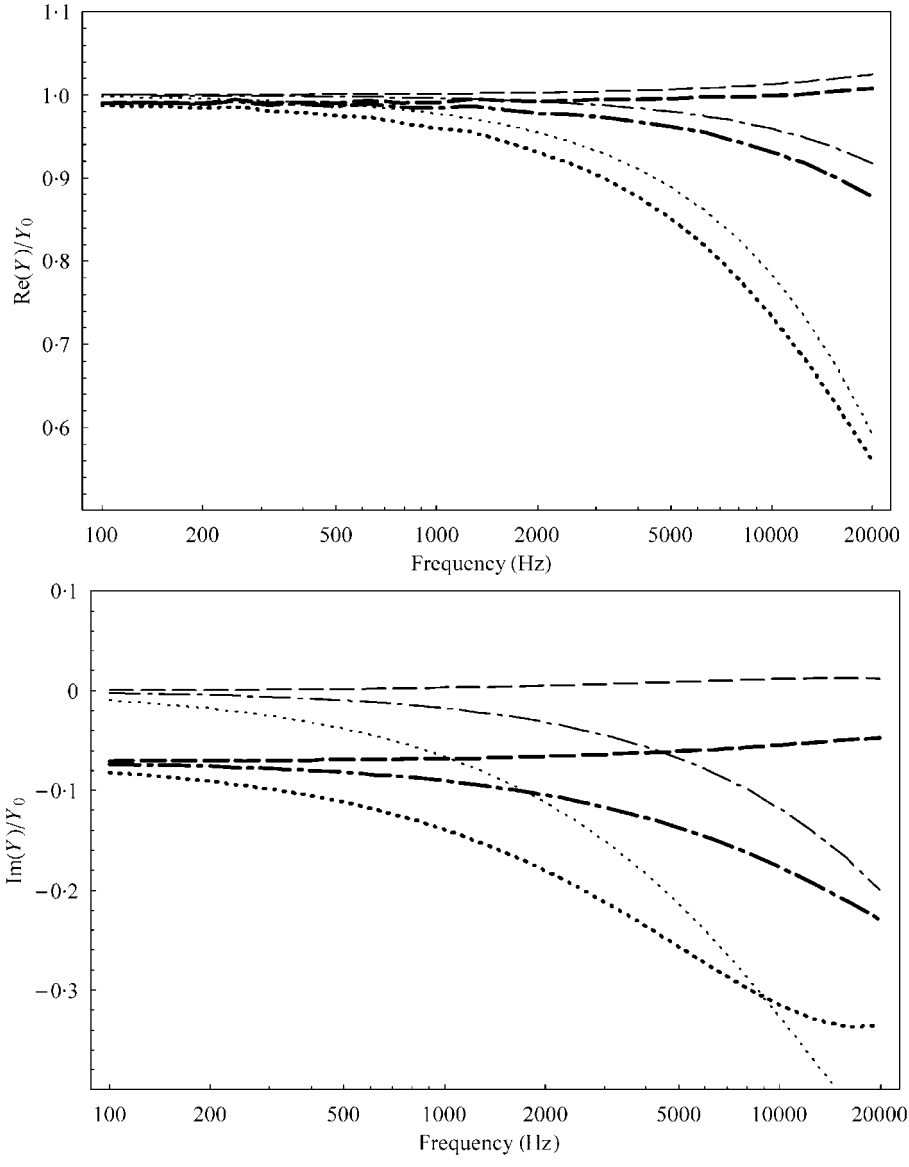

Figure 4. Real (top) and imaginary (bottom) parts of the mobility, normalized with respect to $Y_0 = 1/8\sqrt{B'm''}$. – – –, $a = 2$ mm; – · – $a = 5$ mm; ⋯, $a = 10$ mm; thin lines: equation (47); thick lines; numerical results.

to point mobility calculations. Lamb [9] calculated the out-of-plane point force mobility, while Goyder and White [10] added two point moment mobilities. No results are available for the remaining three point mobilities Y_{P11}, Y_{P33} and Y_{P55}. In terms of a junction, a beam-stiffened plate is equivalent to one beam and two semi-infinite plates with a subtended angle of 180°. The second structure which is studied here adds a perpendicular plate to the beam-stiffened plate. Consequently, it consists of three semi-infinite plates and one beam and will be referred to as T-plate with stiffening beam. For this T-plate with stiffening beam no analytical

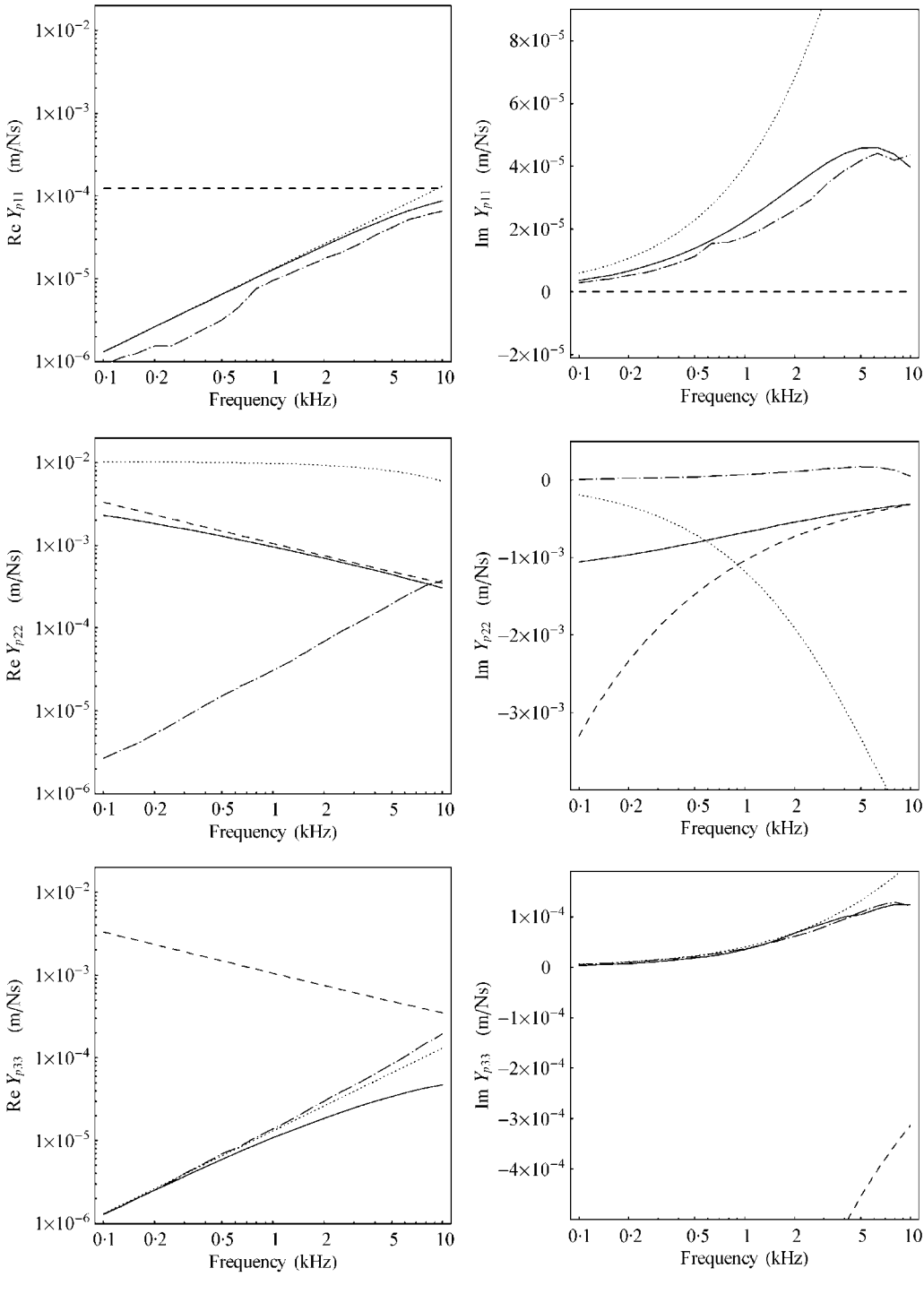

Figure 5. Point force mobilities: ——, beam-stiffened plate; – · –, T-plate; ···, 1 mm steel plate; – – – 10 mm × 10 mm steel beam.

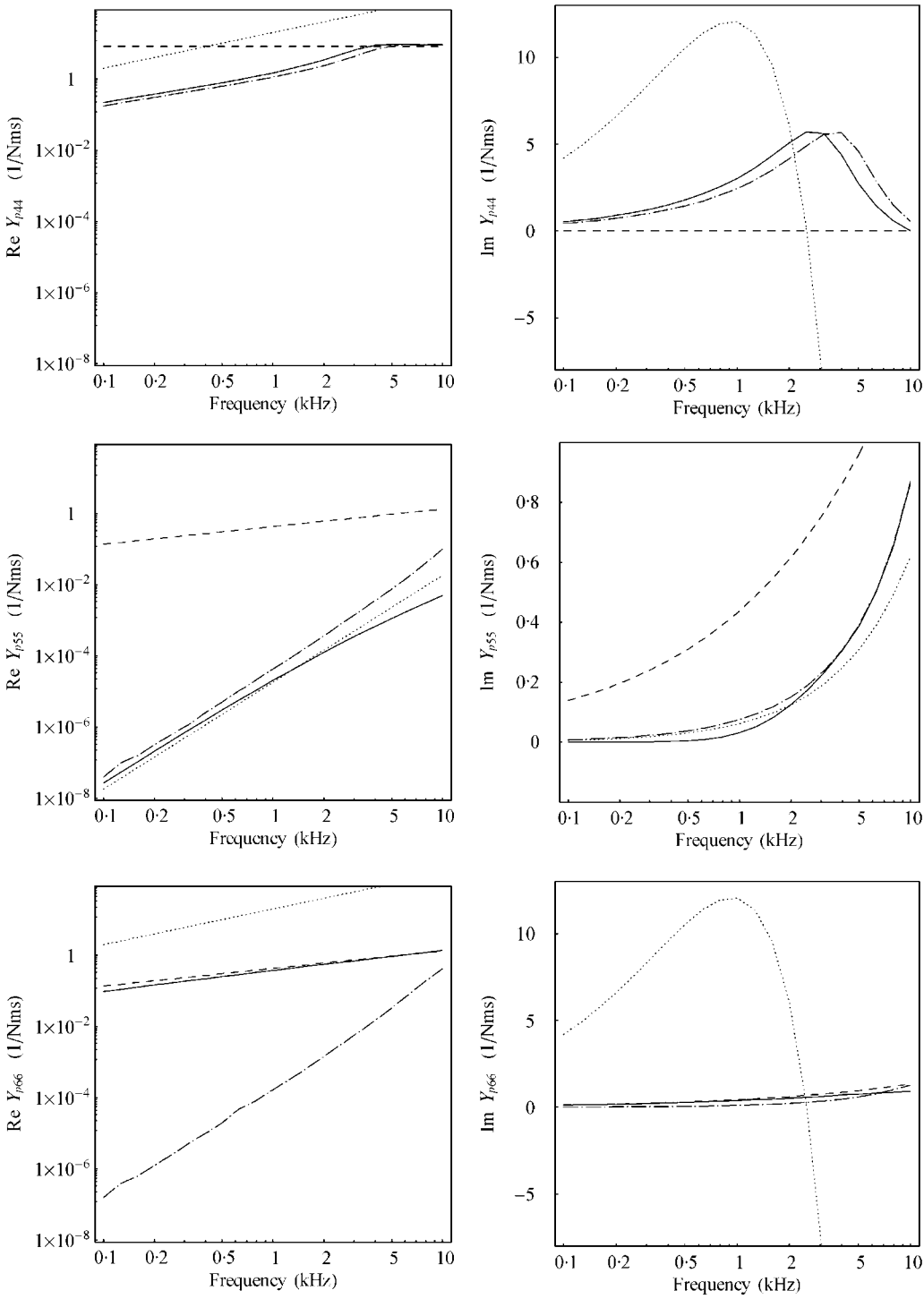

Figure 6. Point moment mobilities (same parameters as in Figure 5).

approximation for point mobilities is available except from that calculated by Petersson [11], which is not applicable in the special case selected here, where relatively thin plates are used and an additional beam is present at the junction.

For both structures all plates were chosen to be 1 mm thick and the beams were set to have a quadratic cross-section of 10 mm × 10 mm. All structural members were taken to be made of steel. The parameter a was chosen to be 10 mm, while as well as in the first example interpolating functions of degree $p = 7$, $q = 8$ were shown to be best suited for the numerical calculation. Figure 5 shows the results for all point force mobilities for both structures, while Figure 6 shows the point moment mobilities. Along with the real and imaginary parts of the mobilities from the numerical calculations the analytical results for the point mobilities of a 1 mm steel plate, taken from equations (46)–(49), and for a 10 mm × 10 mm steel beam (see Appendix C) are plotted. The main intention for this was to show that plate and beam formulas give good approximations for the mobilities of this built-up structures in some cases, while in other cases such approximations are rather poor. It may be noticed that the real parts of the mobilities of built-up structures are not very different from those of the member with the lowest mobility. For Y_{P11}, Y_{P33}, Y_{P44} and Y_{P55} the plate governs the behaviour. The real parts of Y_{P22} and Y_{P66} of the beam-stiffened plate and the T-plate are controlled by the beam and the perpendicular plate respectively. The imaginary parts for the built-up structures are different from those of beam and plate in most cases. It seems that no general rule may be established here.

While in most cases the numerical precision of the results is better than 3 digits, in some cases only a precision less than 2 digits was achieved in calculation. These less-precise results had also to be used for plotting the curves in Figures 5 and 6, so it is due to a technical but not a physical reason that some curves (most notable Y_{P11} of the T-plate) appear to be not smooth.

Even though not shown here the numerical results for the beam-stiffened plate were also compared to the results from references [9, 10]. The agreement is good except for Y_{P44}, where an obvious misprint in reference [10] leads to notable differences.

6. CONCLUDING REMARKS

This work has been concerned with how to compute point mobilities of complicated structures, in particular generic multi-plate/beam junctions. It has been shown that an algorithm which is relatively straightforward may be used to calculate the line impedance of the junction from the plate edge impedances and the beam impedance. Together with the wavenumber spectrum of a point force acting this line impedance yields the velocity wavenumber spectrum, which is normalized and integrated to get the point mobility. This integration has to be done numerically. A specially adapted integration technique was introduced to reduce the required amount of numerical calculation.

The foremost theoretical imitation of the technique is that the indenter is assumed to be line-shaped. This affects mainly the values of the imaginary part of

the mobility. The effect of the numerical errors arising during computation requires careful consideration as it may result in imprecise or even totally meaningless results.

The successful calculation of the point mobilities of an infinite homogenous plate shown in the work suggests that the method's results are reliable. Demonstrating its potentials, the method was also employed to more complicated structures.

Throughout the present analysis only homogenous plates and the stiffening beam were considered as structural members of the junction. The analysis may readily be extended to include other types of structural members, if their edge impedance or dynamic stiffness can be estimated (e.g. cylindrical shells [17]). Furthermore, the method allows in principle the inclusion of material damping and of elastic interlayers between the plates and the beam.

ACKNOWLEDGMENTS

The author wishes to thank Prof. W. Wöhle for his consistent guidance and many helpful discussions throughout the last years.

REFERENCES

1. L. Cremer and M. Heckl 1996 *Körperschall*. Berlin: Springer-Verlag, second edition.
2. I. Dyer 1960 *Journal of the Acoustical Society of America* **32**, 1290–1297. Moment impedances of plates.
3. E. Eichler 1964 *Journal of the Acoustical Society of America* **36**, 344–348. Plate-edge admittances.
4. T. Beckmann 1977 *Dissertation, Technische Universität Dresden*. Beiträge zur Anwendung der Statistischen Energieanalyse für die Berechnung der Körperschalltransmission an Plattenstoßstellen.
5. M. Heckl 1981 *Acustica* **49**, 183–191. Körperschallübertragung bei homogenen Platten beliebiger Dicke.
6. K. J. Buhlert 1981 *Journal of Sound and Vibration* **78**, 235–245. Driving point impedances of thick homogeneous plates in flexure.
7. S. Ljunggren 1984 *Journal of Sound and Vibration* **93**, 161–187. Generation of waves in an elastic plate by a torsional moment and a horizontal force.
8. R. C. N. Leung and R. J. Pinnigton 1986 *Journal of Sound and Vibration* **111**, 125–129. Point inertance of an infinite plate with respect to a force acting in its plane.
9. G. L. Lamb 1961 *Journal of the Acoustical Society of America* **33**, 628–633. Input impedance of a beam coupled to a plate.
10. H. G. D. Goyder and R. G. White 1980 *Journal of Sound and Vibration* **68**, 75–96. Vibrational power flow from machines into built-up structures, Part II: wave propagation and power flow in beam-stiffened plates.
11. B. Petersson 1983 *Journal of Sound and Vibration* **91**, 219–238. An approximation for the point mobility at the intersection of two perpendicular plates.
12. B. Petersson 1984 *Journal of Sound and Vibration* **94**, 495–524. The prerequisites for measuring mobility using annular transducer accessoires.
13. R. S. Langley and K. H. Heron 1990 *Journal of Sound and Vibration* **143**, 241–253. Elastic wave transmission trough plate/beam junctions.
14. B. A. T. Petersson and M. Heckl 1996 *Journal of Sound and Vibration* **196**, 295–321. Concentrated exitation of structures.
15. G. Engeln-Müllges and F. Reutter 1996 *Numerik-Algorithmen*. Düsseldorf: VDI-Verlag.

16. W. H. Press, S. A. Teukolsky and W. T. Vetterling 1993 *Numerical Recipes in C*. Cambridge: Cambridge University Press.
17. R. S. Langley 1994 *Journal of Sound and Vibration* **169**, 297–317. Elastic wave transmission coefficients and coupling loss factors for structural junctions between curved panels.

APPENDIX A: MATRICES FROM SECTION 3.2

$$\mathbf{C} = \begin{pmatrix} \dfrac{k_x}{k_T} & \dfrac{k_{2T}}{k_T} & 0 & 0 \\ 0 & 0 & -1 & -1 \\ \dfrac{k_{zL}}{k_L} & -\dfrac{k_x}{k_T} & 0 & 0 \\ 0 & 0 & -\dfrac{\mathrm{j}k_{zB1}k_{B0}^2}{h_1} & -\dfrac{\mathrm{j}k_{zB2}k_{B0}^2}{h_2} \end{pmatrix},$$

$$\mathbf{Z}'_{FM} = \begin{pmatrix} \dfrac{Ehk_{zL}k_x}{\omega k_T(1+\mu)} & \dfrac{Eh(k_{zT}^2 - k_x^2)}{2\omega k_T(1+\mu)} & 0 & 0 \\ 0 & 0 & \dfrac{m''k_{zB1}(k_{zB1}^2 + (2-\mu)k_x^2)}{\omega h_1} & \dfrac{m''k_{zB2}(k_{zB2}^2 + (2-\mu)k_x^2)}{\omega h_2} \\ -\dfrac{Eh(k_{zL}^2 + \mu k_x^2)}{\omega k_L(1-\mu^2)} & \dfrac{Ehk_{zT}k_x}{\omega k_T(1+\mu)} & 0 & 0 \\ 0 & 0 & \dfrac{\mathrm{j}m''(k_{zB1}^2 + \mu k_x^2)}{\omega h_1} & \dfrac{\mathrm{j}m''(k_{zB2}^2 + \mu k_x^2)}{\omega h_2} \end{pmatrix}$$

$$k_{zB1/2} = \mathrm{j}\sqrt{k_x^2 - k_{B1/2}^2}, \quad k_{zL} = \mathrm{j}\sqrt{k_x^2 - k_L^2}, \quad k_{zT} = \mathrm{j}\sqrt{k_x^2 - k_T^2},$$

$$h_{1/2} = k_{S\kappa}^2 k_{B1/2} - k_L^2 k_{Sk}^2 + k_{B0}^2.$$

APPENDIX B: BEAM IMPEDANCE MATRIX

The non-zero elements of $\mathbf{Z}'_{KB}$ are

$$Z'_{KB11} = \mathrm{j}\left(\omega m' - \frac{k_z^2 L}{\omega}\right), \quad Z'_{KB22} = \mathrm{j}\left(\omega m' - \frac{k_z^2 K_y}{\omega}\right), \quad Z'_{KB24} = Z'_{KB42} = \mathrm{j}\omega m' z_S,$$

$$-Z'_{KB26} = Z'_{KB62} = \frac{k_z K_y}{\omega}, \quad Z'_{KB33} = \mathrm{j}\left(\omega m' - \frac{k_z^2 K_z}{\omega}\right),$$

$$Z'_{KB34} = Z'_{KB43} = -\mathrm{j}\omega m' y_S,$$

$$Z'_{KB35} = -Z'_{KB53} = \frac{k_z K_z}{\omega}, \quad Z'_{KB44} = \mathrm{j}\left(\omega\Theta'_x - \frac{k_z^2 G J_{Sx}}{\omega}\right),$$

$$Z'_{KB55} = \mathrm{j}\left(\omega\Theta'_y - \frac{k_z^2 B_y}{\omega} - \frac{K_z}{\omega}\right), \quad Z'_{KB66} = \mathrm{j}\left(\omega\Theta'_z - \frac{k_z^2 B_z}{\omega} - \frac{K_y}{\omega}\right).$$

APPENDIX C: POINT MOBILITY OF AN INFINITE BEAM

Point mobilities of an infinite beam [1] (Timoshenko bending theory):

$$Y_{P11} = \frac{1}{2S\sqrt{E\rho}}, \quad Y_{P22} = \frac{\omega^2\rho/G + k_{Bz1}k_{Bz2}}{2\omega m'(k_{Bz1} + k_{Bz2})}, \quad Y_{P33} = \frac{\omega^2\rho/G + k_{By1}k_{By2}}{2\omega m'(k_{By1} + k_{By2})},$$

$$Y_{P44} = \frac{1}{2J_{Sx}\sqrt{G\rho}}, \quad Y_{P55} = \frac{(1 + \mathrm{j}\omega)}{4k_{By1}EI_y}, \quad Y_{P66} = \frac{(1 + \mathrm{j}\omega)}{4k_{By1}EI_z}.$$

$k_{By1/2}$ and $k_{Bz1/2}$ are the wavenumbers for free bending waves on the beam and can be estimated like those for the plate (equation (14)).